ISSN 0010-5082, Combustion, Explosion, and Shock Waves, 2018, Vol. 54, No. 4, pp. 450–460. © Pleiades Publishing, Ltd., 2018.
Original Russian Text © A.N. Pivkina, N.V. Muravyev, K.A. Monogarov, D.B. Meerov, I.V. Fomenkov, E.A. Skryleva, M.Yu. Presnyakov, A.L. Vasiliev, N.I. Shishov, Yu.M. Milekhin.

Comparative Analysis of Boron Powders Obtained by Various Methods. I. Microstructure and Oxidation Parameters during Heating

A. N. Pivkina[a], N. V. Muravyev[a], K. A. Monogarov[a], D. B. Meerov[a], I. V. Fomenkov[b], E. A. Skryleva[c], M. Yu. Presnyakov[d], A. L. Vasiliev[d], N. I. Shishov[e], and Yu. M. Milekhin[e]

UDC 662.7+546.1+536.46

Published in *Fizika Goreniya i Vzryva*, Vol. 54, No. 4, pp. 73–83, July–August, 2018.
Original article submitted July 10, 2017; revision submitted August 18, 2017.

Abstract: This paper describes a study of boron powders and powder compounds, obtained by various methods, including metallothermal, electrolytic, and borane cracking methods. The crystal state, particle size and microstructure, presence and composition of impurities, and chemical composition of the oxide layer of boron particles are profoundly investigated. The effects of the above-mentioned characteristics on the particle oxidation parameters during heating with a constant rate are analyzed. The determining influence of chemical composition of the particle surface layer on the initial temperature of their intense oxidation is established. It is shown that the maximum increase in the mass and heat release value during oxidation of the boron powders is almost independent of microstructural features, crystal state, and chemical composition of and oxide layer thickness of the particles, and cannot serve as indicators of completeness of boron oxidation during heating.

Keywords: boron particles, boron production, microstructure, boron oxidation, thermal analysis.

DOI: 10.1134/S0010508218040093

INTRODUCTION

As is known, powdered boron is one of the most promising components of pyrotechnic compositions and solid fuels for various purposes [1] as its combustion heat is the largest among all elements per unit volume (140 kJ/cm^3) and the third largest per unit mass (59 kJ/g), behind hydrogen and beryllium. The indicated values in the calculation exceed similar values for hydrocarbon fuels 3 times with respect to the unit volume and 1.4 times with respect to the per unit mass [2].

Despite such a high potential, the practical use of boron particles in high-energy compositions is often accompanied by a low completeness of their combustion and, as a result, reduced efficiency of propulsion devices. The main reason is the peculiarities of the combustion of boron particles, among which one can distinguish several phenomena. Firstly, difficulty of ignition of solid boron particles, which is explained by the fact that a solid boron core is covered by a molten layer of boron

[a]Semenov Institute of Chemical Physics, Russian Academy of Sciences, Moscow, 119991 Russia; alla_pivkina@mail.ru.
[b]Zelinsky Institute of Organic Chemistry, Russian Academy of Sciences, Moscow, 119991 Russia.
[c]National University of Science and Technology "MISiS," Moscow, 119049 Russia.
[d]National Research Center "Kurchatov Institute," Moscow, 123182 Russia.
[e]Federal Center for Dual-Use Technologies "Soyuz," Dzerzhinsky, 140090 Russia.

oxide at temperatures above 450°C (the boiling point is 1860°C). Secondly, prevention of boron combustion in a gas phase due to its high boiling point (3865°C at a pressure of 0.1 MPa) and slower heterogeneous reactions of its oxidation on the surface [3]. Thirdly, boron particles are highly inclined to forming agglomerates during heating, which is associated with the presence of a molten layer on the particle surface, which increases the burning time of boron particles (as a rule, particles with a diameter of 100 μm burn out for 20–30 ms [2]) and increases this time in comparison with the time the fuel spends in the combustion chamber of the engine.

Thus, in compositions based on ammonium perchlorate, inert binder, and 15.7% ALEX aluminum, the replacement of 2% of metal by ultradisperse boron does not change the burning rate and substantially increases the degree of agglomeration of aluminum [4].

These difficulties can be overcome and the completeness of oxidation and combustion of boron can be increased by adding rare earth metals [5], magnesium [6], and metal hydrides [7]. The catalytic effect of metal oxides (Bi_2O_3, Fe_2O_3, and Al_2O_3) on the onset temperature drop is determined in [8]. Another direction is the decreasing size of boron particles. Nanosized boron particles are obtained, for example, by the thermolysis of diborane at a temperature of 700–2250°C [9] and reduction of boron from boron trichloride by hydrogen [10] or sodium naphthalene [11]. For boron nanoparticles, the ignition delay time decreases and the completeness of combustion increases as compared to micron-size particles [12, 13].

Boron oxidation during heating with a rate of tens of degrees per minute (thermoanalytical measurements) and millions of degrees per minute (combustion) depend on the powder dispersion in different ways. Thus, the temperature at the beginning of the intense oxidation of boron during slow heating in an oxidizing medium is almost independent of the particle size, and the maximum mass gain paradoxically increases with increasing particle size [14, 15]. In [15], the crystalline boron powder is divided into fractions and the mass gain, referred to a theoretically possible value, is determined during heating in an oxidizing medium. It turns out that, with an increase in the average size of the fraction from 25 to 65 μm, this value increases from 64 to 79%.

The burning rate of boron-containing compositions increases linearly with increasing contact surface of boron particles with an oxidant per unit volume of fuel, as is described in [16].

It is experimentally shown [17] that fluorine removes the oxide layer on boron particles, which results in the fact that the delay time of their ignition decreases and the burning rate increases. However, it is certain that using fluorine-containing fuel does not lead to the mentioned effects [18], while the modification of the particle surface by removing the oxide layer [19] or introducing the functional fluorine-containing groups on the particle surface [20–22] significantly changes the parameters of oxidation and combustion of boron particles.

Starting with the first works on the study of combustion of boron particles [23–25] and ending with more modern works [26, 27], the objects of study are usually micron-sized particles of crystalline boron. However, the particles of amorphous boron are more active chemically in oxidation and combustion than crystalline boron. This is indicated by the experimental data: during the transition from crystalline to amorphous boron, the effective energy of oxidation activation falls from 297 to 191 kJ/mol, the delay time of ignition decreases too, and the intensity of the emission spectrum during combustion increases [27].

The size distribution, crystalline state, microstructure, impurities, chemical composition, and thickness of the surface layer of boron particles are the factors which affect the oxidation and combustion of boron as part of high-energy compositions and are determined by the method of the boron powder synthesis. Currently, the following common methods are distinguished. Firstly, a magnesium-thermal method which comes down to reducing B_2O_3 by metallic magnesium. Secondly, cracking of borohydrides which is based on the thermal decomposition of boranes as they pass through a heated quartz tube. Thirdly, an electrolytic method for obtaining boron particles.

The analysis of the literature data shows that the information on the effect of the synthesis method of boron on the processes of oxidation and combustion are shown fragmentarily, with no systematic studies available.

The purpose of the paper is to determine the relationship between the crystalline state, particle size, microstructure, chemical composition, and oxide layer characteristics of boron particles with the parameters of their oxidation under nonisothermal heating with constant velocity. In subsequent works, the results of the study of the kinetic laws of physical and chemical processes in non-isothermal oxidation, as well as the results of the study of physical and chemical processes in the combustion of boron-containing high-energy compositions will be reported.

1. EXPERIMENT

Four samples of powdered boron, synthesized by different methods (Table 1), are under study. Amorphous boron (sample No. 1) is obtained by cracking of

Table 1. Samples and methods for obtaining them

Sample number	Sample	Synthesis method
1	Amorphous boron	Cracking of boranes
2	Magnesium polyboride	Metallothermal
3	Aluminum polyboride	Metallothermal
4	Electrolytic boron	Electrolysis

borohydrides as they pass through a quartz tube at a temperature above 700°C. The boron synthesized this way is deposited on the walls of the tube in the form of a thin layer of powder, and the particles obtained are usually characterized by a quasispherical shape and smooth surface [20]. Magnesium polyboride (sample No. 2) is produced by metallothermal technology (Moissan's method), contains amorphous boron, β-rhombohedral modification of boron, and magnesium borides, and consists of 85% of boron and up to 10% of magnesium (by mass) according to the manufacturer's information [28]. Aluminum polyboride (sample No. 3) is also synthesized by the metallothermy method (Moissan's method) [28]. Electrolytic boron (sample No. 4) is obtained by electrolysis from a melt that contains KCl (70%), KF (12%), and potassium fluoroborate KBF_4 (18%). Electrolysis is carried out in a graphite crucible that serves as an anode by using a steel cathode at 800°C, and the boron removed from the cathode after purification is grinded in a ball mill [29]. The resulting boron powder, according to the literature, has the form of the β-rombohedral modification crystals surrounded by amorphous boron particles [30].

The particle size distribution is determined by the method of dynamic laser diffraction on Analysette 22 MicroTec Plus (Fritsch) in water with the addition of a surfactant and with pre-treatment by ultrasound to separate the aggregated particles of the powder. For each powder, at least five samples are taken, with each analyzed at least five times.

The specific surface area of the samples is determined using FlowSorb III 2305 (Micromeritics) by measuring nitrogen adsorption on the powder surface, with at least three measurements for each sample, while the reproducibility of the measurement results is not less than 99.5%.

The sample composition is studied via x-ray diffraction with the help of a D8 ADVANCE (Bruker) diffractometer equipped with a nickel β filter, a system of controlled slots for monochromatization ($\lambda[\mathrm{Cu}K_\alpha] = 1.5418$ Å), and a position-sensitive Lynx-Eye detector in a range of angles of 4–80° with a step of 0.02° in the angle 2θ. The diffraction data are processed and the calculations are carried out using EVA (Bruker) and TOPAS 4.2 (Bruker) software.

The morphology and microstructure of the particles are investigated using a Quanta 3D FEG (FEI) Scanning Electron–Ion Microscope and a TITAN 80-300 TEM/STEM (FEI) Transmission/Scanning Electron Microscope at an accelerating voltage of 300 kV. The device is additionally equipped with a high-angle circular dark-field detector (Fishione), an energy-dispersion x-ray spectrometer (EDAX), and a Gatan image filter (GIF, Gatan), the latter of which is used to identify elements with small atomic numbers (boron, carbon, oxygen, and nitrogen). All images are processed using Digital Micrograph (Gatan) and TIA (FEI) software.

The elemental and chemical analysis of the particle surface is determined by the x-ray photoelectron spectroscopy (XPS) method on a 5500 VersaProbe II (PHI) spectrometer. Photoemission is excited by using a monochromatic $\mathrm{Al}K_\alpha$ radiation ($h\nu = 1\,486.6$ eV) with a power of 50 W. The samples of boron powders are pressed into a continuous layer of indium foil with an area of about 0.5 cm^2, and the diameter of the analyzed region is 200 μm. The atomic concentrations are determined by the relative elemental sensitivity factor with the use of values from the PHI database. The high resolution spectra are taken with the transmission energy of the analyzer equal to 11.75 eV and a data acquisition density of 0.1 eV/step. The high-resolution spectra are processed by approximating their using the nonlinear least-squares method with help of the Gauss–Lorentz function. Adsorbed impurities are removed by means of etching by Ar^+ ions with an energy of 2 keV, a (2 ×2)-mm raster, and an etching rate determined on the SiO_2 layer as 2 nm/min.

The thermal behavior of the samples in the air flow is studied by means of synchronous thermal analysis (STA) on STA 449 F3 (Netzsch) at a heating rate of 10 K/min. The measurements are carried out both in oxidizing (air flow of 100 ml/min) and inert (argon flow of 70 ml/min) media.

2. RESULTS AND DISCUSSION

According to the results of laser diffractometry of the boron samples under study, the particle size of the powders does not exceed 20 μm, which agrees with the measured values of the specific area of the surface within $S_{\mathrm{sp}} = 5$–10 m^2/g (see Table 2 and Fig. 1). The particle size distribution for sample Nos. 1 and 4 is monomodal, and the mass-average diameter of the

Table 2. Particle size and specific surface of samples

Sample number	S_{sp}, m^2/g	D_{43}, μm	D_{10}, μm	D_{50}, μm	D_{90}, μm
1	7.2 ± 0.2	3.2 ± 0.2	0.5 ± 0.1	2.2 ± 0.1	7.4 ± 0.6
2	4.7 ± 0.1	8.1 ± 0.5	1.0 ± 0.1	6.5 ± 0.3	17.0 ± 0.4
3	5.2 ± 0.1	4.5 ± 0.2	0.5 ± 0.1	2.3 ± 0.1	12.9 ± 0.6
4	10.0 ± 0.2	2.3 ± 0.2	0.35 ± 0.03	1.29 ± 0.07	4.9 ± 0.5

Table 3. Composition of the crystalline phase of the samples

Sample number	β-B, %		AlB_{31}, %	BN, %	Silicon, %	H_3BO_3, triclinic modification, %
	rhombohedral	tetragonal				
1	—	—	—	—	—	—
2	83.8	15.9	—	—	0.2	0.1
3	19.1	—	80	—	—	0.2
4	82.9	17.1	—	—	—	—

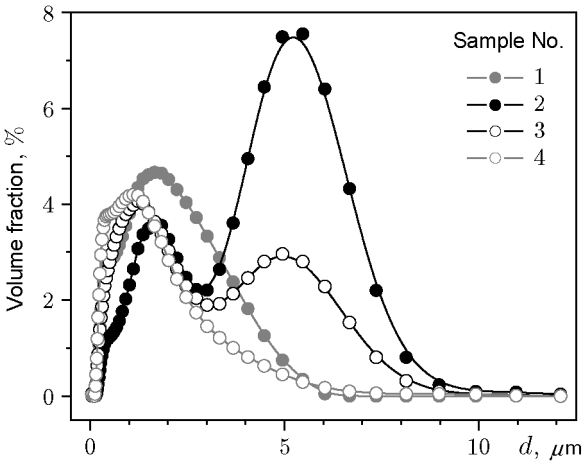

Fig. 1. Size distribution of boron particles.

particles is D_{43} = 2–3 μm. At the same time, in the case of the boron sample Nos. 2 and 3, there could be an additional mode ≈5 μm, which increases D_{43} up to 4–8 μm.

The x-ray analysis of powder 1 shows no crystalline peaks, i.e., the sample is amorphous. In the spectra of sample Nos. 2–4, the crystalline phases of boron rhombohedral and tetragonal modifications (Table 3) are revealed.

According to the scanning electron microscopy (SEM), sample No. 1 has the form of conglomerates of up to 10 μm in size, which do not have a noticeable amorphous covering (Fig. 2). This confirms the assumption made in [25] on the absence of an oxide shell on the particles of amorphous boron. The observed conglomerates are formed by spherical submicron particles with a smoothed surface. The particles with diameters larger than 2 μm often contain spherical cavities in the volume, which are formed apparently during synthesis. The energy-dispersive x-ray microanalysis shows that, in addition to boron, the samples also contain oxygen.

The crystallites of sample No. 2 with a size of up to 600 nm are covered by an amorphous layer 1–5 nm in thickness and form large (up to 80 μm) conglomerates of irregular shapes (Fig. 3). The structure of these crystallites corresponds to a hexagonal crystal lattice, and the interplanar distances estimated from high-resolution SEM spectra turn out to be somewhat larger than those for β-B [31]. Thus, taking into account the high content of Mg in the particles, it can be assumed there is the presence of $B_{19.046165}Mg_{0.971}$ magnesium boride [32]. The basic elements determined in the sample are boron, oxygen, and magnesium.

The boron particles of sample No. 3, which are different in their morphological structure and composition, also form conglomerates. Thus, the typical sample contains the following components. Firstly, faceted and spherical particles with a diameter of about 1 μm with a non-smooth terraced surface (Fig. 4a). Secondly, faceted submicron particles of β-B (Fig. 4b) with no surface amorphous oxide layer. Thirdly, amorphous particles of irregular shapes (Fig. 4b). Fourthly, aluminum

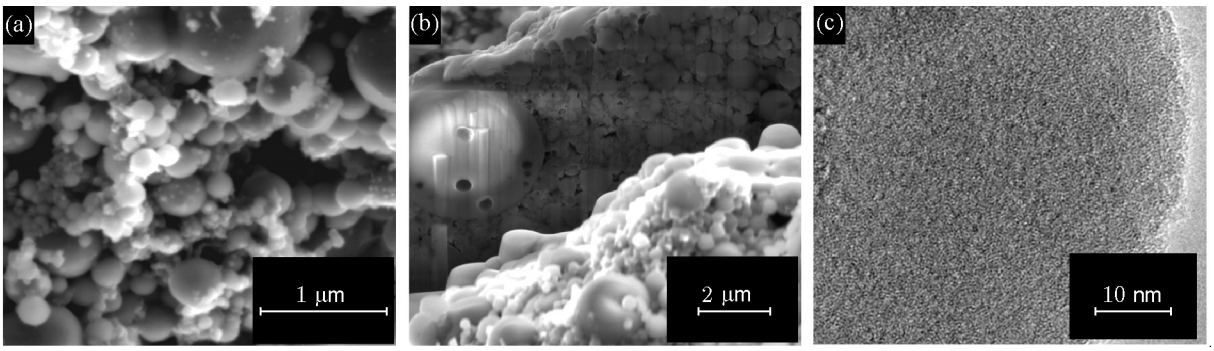

Fig. 2. SEM images of the particles of sample No. 1: (a) conglomerate of submicron particles; (b) cross section of the particle conglomerate, with spherical cavities inside; (c) amorphous structure of the particles.

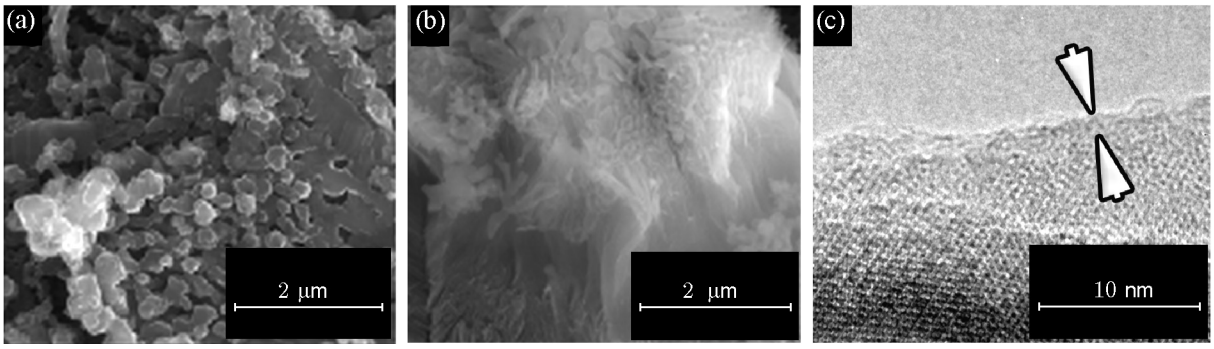

Fig. 3. SEM images of the structure of sample No. 2: (a) conglomerate of the submicron particles; (b) image of the particle surface; (c) amorphous surface shell.

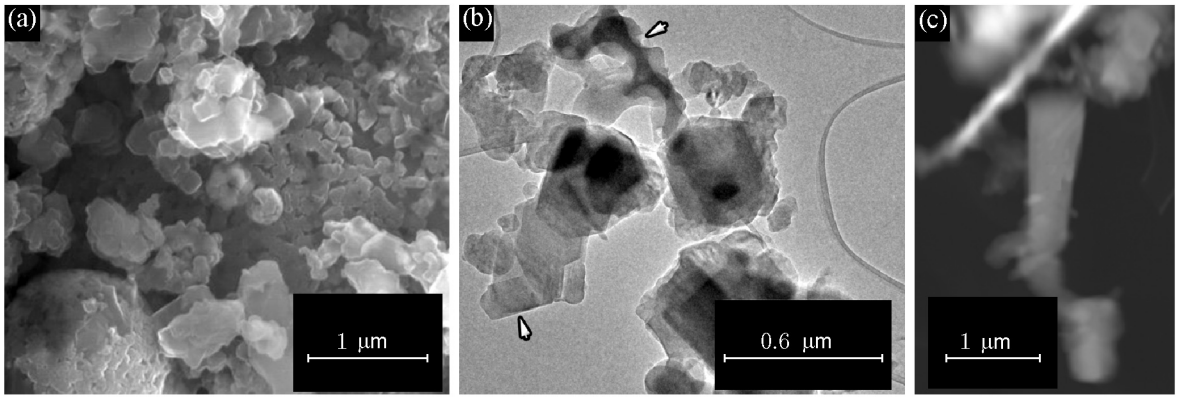

Fig. 4. SEM image of the morphology of sample No. 3: (a) conglomerates consisting mainly of crystallites with a faceting of submicron and micron sizes; (b) light-field TEM image; (c) dark-field image of an aluminum boride particle (in the center).

boride particles (Fig. 4c). The latter correspond to the $Al_{6.3}B_{88}$ phase of the space group $P2_12_12_1$ with the following unit cell parameters: $a = 1.65$ nm, $b = 1.75$ nm, and $c = 1.01$ nm [33]. The XRD of bulk powder (see Table 1) establishes the presence of a AlB_{31} phase a similar structure, which is formed by the β-rombohedral modification of boron with inclusions of aluminum atoms in the unit cell.

Sample No. 4 consists of the β-B particles of the rhombohedral modification, which can morphologically be divided into three types (Fig. 5): particles of irregular shapes with size of up to 5 μm (group A), elongated

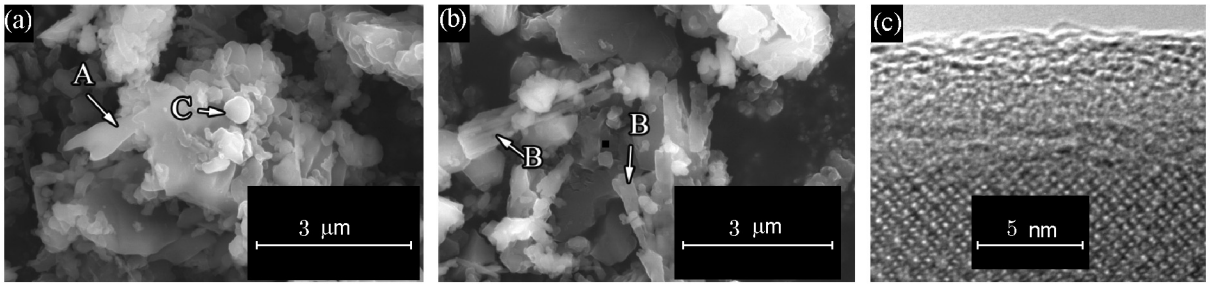

Fig. 5. SEM image of the particles of sample No. 4 of different morphology (a) and (b) and the oxide layer on the particle surface (c).

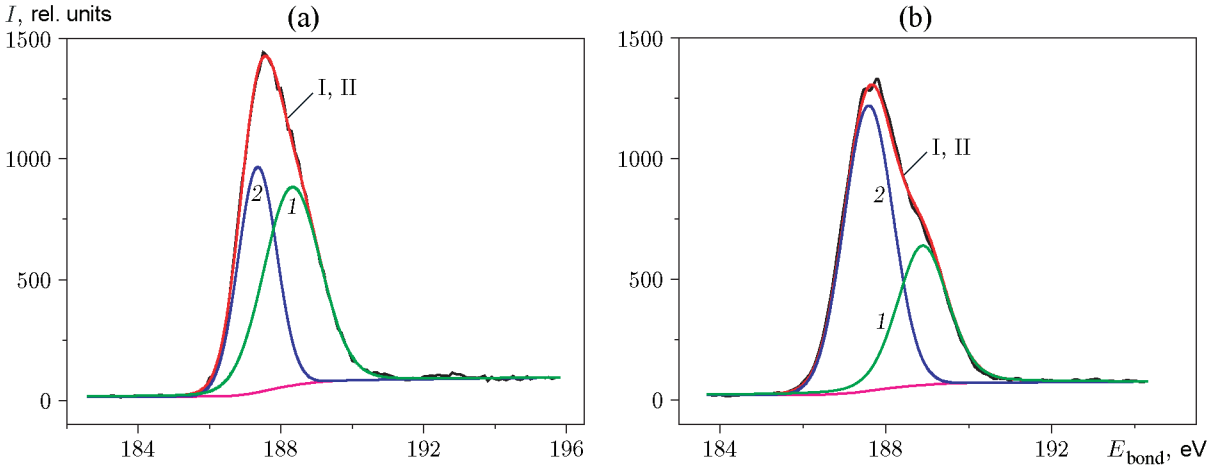

Fig. 6. Spectra of the $B1s$ sample Nos. 1 (a) and 4 (b): I and II are the experimental synthetic spectrums, respectively; *1* and *2* are the simulated peaks of elementary boron and B_6O, respectively.

particles with a size of 1–10 μm (group B), and spherical diameters of about 0.3 μm (group C). The thickness of the amorphous layer on the surface of these particles varies from 1 to 5 nm (Fig. 5c).

X-ray photoelectron spectroscopy (XPS) is used to determine the elemental composition of the surface of the boron samples under study. Note that the data represent averaging over the depth of the sample equal to 2–3 nm (an estimate based on the mean free path of photoelectrons for the $B1s$ level).

On the surface of all samples, the dominant element is boron, and oxygen, nitrogen, magnesium, aluminum, and potassium can be found in noticeable amounts. Moreover, the concentration of the impurity elements significantly is reduced after ion etching. Thus, the particles are a core of metallic boron coated with an impurity-containing oxide layer. It is known that some level of impurities is retained in etching of powdered samples of boron, while etching of a boron single crystal completely removes impurities from an ideal flat surface [34].

The approximation of experimental high-resolution spectra of $B1s$ boron shows that the spectrum consists of two or more components (Fig. 6). Thus, in sample Nos. 1 and 4, the spectrum of $B1s$ consists of peak *1* with a binding energy of 187.2–187.9 eV, which corresponds to the elementary boron [35–37], and peak *2*, whose binding energy (188.2 eV) corresponds to $B_{12}O_2$ or B_6O suboxides [35]. Note that boron powders can contain up to 2% (by weight) of oxygen in the compounds not described by the formula B_2O_3 [38].

As a rule, a B_2O_3 oxide layer is formed on the surface of pure boron, which is manifested in the spectrum of $B1s$ as a peak in a region of 192.4 eV [35]. It is interesting that, for sample Nos. 1 and 4, there is no signal in this region, but there are peaks of bond energy corresponding to the presence of a B_6O suboxide. For sample No. 1 obtained by cracking of boron hydrides, there is possibly $B_{10}H_{14}$ boron hydride with a bond energy of 187.8 eV [39]. The methods of analysis used in this work cannot uniquely determine the presence of hydride on the surface of samples 1. The results of the analysis of

Table 4. Results of the XPS spectra analysis

Sample number	Parameters	$B1s$			$O1s$	$A12p$	$F1s$
		B^0	B_6O	B_2O_3		$Al(OH)_3$	MgF_2
1	E_{bond}, eV	187.3	188.3	—	532.5	—	—
	ε, %	45	55	—	100	—	—
2	E_{bond}, eV	187.5	188.8	192.8	532.5	—	—
	ε, %	38	40	22	100	—	—
3	E_{bond}, eV	187.4	—	192	532.0	74.3	—
	ε, %	90	—	10	—	100	—
4	E_{bond}, eV	187.5	188.7	—	532.2	—	685.6
	ε, %	64	36	—	100	—	100

Table 5. Results of the determination of elemental and chemical compositions of the particles, the thickness of the amorphous layer (δ) and the oxidation process parameters

Sample number	In the volume of the particles				On the surface of the particles												Oxidation		
	Elemental composition, % (by weight)				δ, nm	Elemental composition, % (by weight)						Chemical composition, % (by weight)						T_0, °C	Q, $\frac{kJ}{g}$	Δm, %
	B	O	Mg	Al		B	O	Mg	Al	N	F	B^0	B_6O	B_2O_3	MgF_2	$Al(OH)_3$	MgO			
1	96.9	3.1	—	—	0	83.5	14.3	—	—	2.2	—	39.6	60.4	—	—	—	—	590	15.0	157
2	95.1	1.0	3.6	—	1–5	48.6	44.9	3.9	—	2.6	—	22.2	28.8	40.7	—	—	8.3	743	15.9	126
3	92.1	1.5	0.3	6.1	0–1	49.9	28.2	—	21.2	0.7	—	44.5	—	16.0	—	39.5	—	765	17.8	153
4	98.6	1.4	—	—	1–5	75.8	14.3	0.2	—	0.5	6.4	52.0	36.4	—	11.2	—	0.4	598	11.3	118

Sample No. 2 is the Fe, Pb, and Si impurities, and sample No. 3 is the Fe, Si, Cu, and Mn impurities.

the high-resolution spectra of $B1s$, $O1s$, and $A12p$ of the investigated samples (bond energy E_{bond}, relative intensity of peaks in the spectrum ε, and the interpretation of individual peaks) are presented in Table 4.

The surfaces of sample Nos. 1 and 2 have a B_6O suboxide and a B_2O_3 oxide, respectively. The surface of sample No. 3 could contain a large amount of aluminum in the form of an $AlO_x(OH)_y$ in addition to B_2O_3. As a result of ion etching, the y/x ratio decreases, indicating a transition from a hydro-oxide to an oxide. The B_6O suboxide is found in the oxide shell of sample No. 4 along with a significant amount of fluorine and impurities of magnesium and potassium. The spectrum of $F1s$ is located in the region of 685.6 eV, which corresponds to fluorine in the MgF_2 compound (684.4 eV [40] and 685.75 eV [41]).

Based on the data obtained, the chemical composition of the initial surface of the samples is calculated, and the main chemical compounds are presented in Table 5. The nitrogen observed on the panoramic spectra seems to correspond to the adsorbed nitrogen.

The oxidation of boron samples is studied by means of differential scanning calorimetry (DSC method) and thermogravimetry (TG method) with linear heating (Fig. 7). Table 5 presents the main oxidation parameters: T_0 is the onset temperature of intense oxidation, Q is the heat release during the sample oxidation, and Δm is the increment in the mass of the sample upon oxidation to a temperature of 1100°C. The noticeable oxidation of sample Nos. 1 and 4, accompanied by a mass gain, is observed at a temperature above 600°C. At ≈700°C the mass increasing rate drops both due to the liquid oxide layer thickness growth followed by the slowing of the diffusion rate and the oxide covering evaporation [42]. The evaporation rate stronger depends on temperature than the oxidation one, and at certain point the mass increasing process becomes linear [43,44]. The recorded dependences of the heat re-

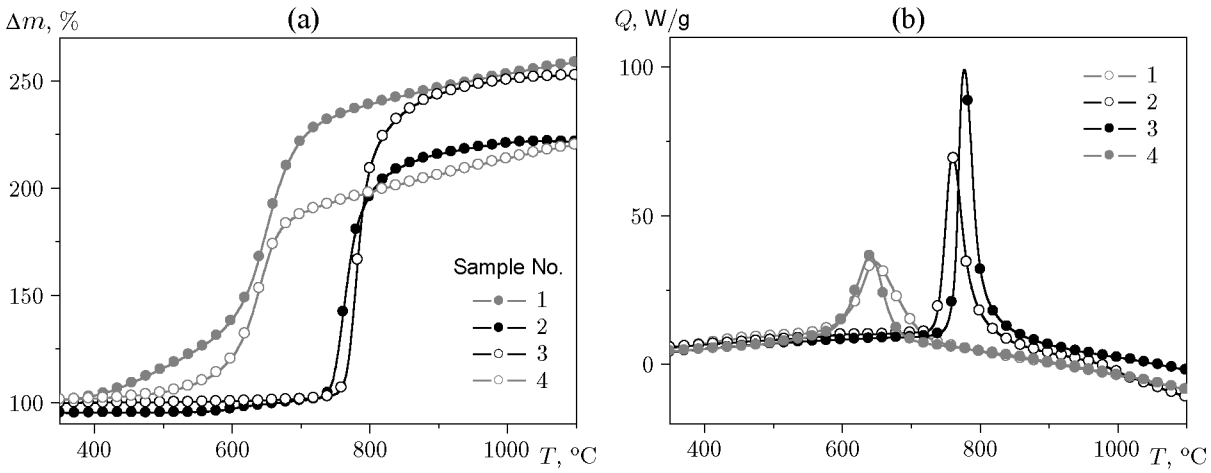

Fig. 7. Oxidation of boron samples during linear heating in an air flow: (a) sample masses vs. temperature (TG method); (b) heat dissipation rates vs. temperature (DSC method).

lease rate (DSC) and changes in the sample mass (TG) are obviously integral dependences, which reflect the kinetic laws of the oxidation and evaporation of boron oxide. A similar trend is observed in the oxidation of sample Nos. 2 and 3: oxidation period at a significant rate (starting at about 750°C) is replaced by a period of slow, practically linear increase in the mass. The comparison of the temperature of the start of intense oxidation of powders shows that, at ≈600°C the samples of amorphous 1 and crystalline 4 boron begin to oxidize, and samples 2 and 3, where aluminum or magnesium is present in a significant amount, are oxidized at ≈150°C later. From the comparison with the results of the microstructure analysis, it is determined that the degree of boron crystallinity, its particle size, or the thickness of the oxide layer are not factors determining the value of T_0. A common feature of sample Nos. 1 and 4 is the presence of the suboxide B_6O and virtual absence of impurities on their surface. A common feature of sample Nos. 2 and 3 is the presence of the B_2O_3 oxide and a significant fraction of impurities on the surface.

The high content of boron oxide on the surface of sample No. 2 (over 40%) apparently prevents oxidation of these particles at $T < T_0$. In addition to boron oxide (16%), the surface of the particles of sample No. 3 contains almost 40% of aluminum hydroxide $Al(OH)_3$, which at $T > 575$°C decomposes with the formation of an oxide. Amorphous alumina in the shell undergoes phase transformations [45]. The density of the amorphous oxide is $\rho = 3050$ kg/m^3, γ-Al_2O_3 is formed during crystallization at 550–600°C with a higher density $\rho = 3660$ kg/m^3, and then the polymorphic transition is realized at ≈750°C: γ-$Al_2O_3 \to \delta$, $\theta \to \alpha$-Al_2O_3 ($\rho = 3\,990$ kg/m^3). As a result of phase transitions of aluminum oxide, there are structural changes in the shell with a partial loss of protective properties, which initiate the active oxidation of boron (the "core" of particles).

Heat release in the boron oxidation reaction contributes to the evaporation of an oxide layer, and the experimentally recorded integral result is determined by a balance between the boron oxidation (mass gain of the sample) and evaporation of boron oxide (mass loss of the sample). As a result, the mass gain of sample Nos. 1 and 3 from room temperature to 1 100°C during heating is almost the same despite the differences in the crystalline modifications of boron and chemical compositions of the surface. A much smaller mass gain is observed in sample No. 4, while the content of boron therein is much higher as compared to other samples. Thus, the dependences of the DSC and TG signals on temperature for boron (unlike, for example, aluminum) cannot serve as a criterion of completeness of oxidation. An example of an incorrect estimate of completeness of boron oxidation by mass gain when it is heated in oxygen is an experimentally observed paradoxical increase in the "reaction completeness" with an increase in the particle size of boron [15].

Analysis of the results obtained shows a close relationship between the synthesis method, physicochemical structure, and character of oxidation, which allows predicting the features of the behavior of boron samples in formulations.

Thus, the boron powder 1 synthesized by the cracking of borohydrides, is characterized by the homogeneous distribution of particles with a shape close to spherical. In view of the maximum boron content, the small amount of impurities, and the absence of a no-

ticeable oxide layer, the sample can be named "pure" boron, and its oxidation could be taken as a reference. However, the results of the physicochemical analysis and experiments on thermal desorption (not shown) suggest the presence of bound hydrogen on the particle surface, which can negatively affect the stability of the compositions.

The boron samples obtained by the metallothermic method with the addition of magnesium and aluminum contain these metals in the form of oxide and hydroxide. This state of the surface is evidenced by the XPS data, while the analysis of the crystalline phase of the "volume" of particles reveals only a small amount of Al and Mg bound to boron in a ratio significantly smaller than 1 : 2 or 1 : 12. It is obvious that the introduction of metals into these samples does not contribute to activating the boron ignition in a combustion wave.

However, the unexpected effect of the Al and Mg oxides included in the surface layer on the sample oxidation is revealed. It begins much later than "pure" amorphous boron. It is possible that this effect can lead to changes in the combustion of particles in a two-chamber direct-flow engine and ensures the "delivery" of non-reacted and non-agglomerated boron particles from the gas generator to the combustion chamber [46]. Note that sample No. 4 contains a mixture of MgF_2, which slightly changes the oxidation character of the powder compared with "pure" boron. However, it is known that metal fluorides are catalysts for combustion of energy condensed systems, so the possible influence of MgF_2 on the combustion of compositions requires a separate study.

CONCLUSIONS

The analysis of the boron samples synthesized by various methods used in the industry is described. An interdisciplinary approach was applied based on the results obtained by various physical and chemical methods: x-ray phase analysis, electron microscopy, photoelectron spectroscopy, and thermoanalytical measurements.

The search for factors that affect the oxidation parameters of boron powders, obtained by different methods, shows that the determining effect on the temperature of the start of intensive chemical oxidation is produced by the chemical composition of the surface layer of the particles. In particular, the presence of the B_6O suboxide on the particles of amorphous and electrolytic boron leads to a high chemical activity of these samples in the oxidation reaction and a decrease in the temperature of the start of intense oxidation by 150°C as compared to the samples obtained by the metallothermal method, containing a significant amount of B_2O_3 or Al_2O_3 oxides on the surface.

The maximum mass gain and the amount of heat release during the oxidation of boron powders are practically independent of the microstructural features, crystalline state, chemical composition of the particles, and thickness of their oxide layer and cannot serve as indicators of the completeness of boron oxidation upon heating. Heat release and completeness of the reaction are determined by the superposition of the kinetic laws of boron oxidation and boron oxide evaporation.

The work was carried out with partial financial support of the Russian Foundation for Basic Research (Grant No. 16-29-01055; RFNC, RFA) and at the expense of a grant for executing the state task on the topic 0082-2018-0002, AAAA-A18-118031490034-6 (SEM, STA).

REFERENCES

1. *Ramjet Rocket Engines on Solid and Pasty Fuels. Basics of Design and Experimental Development*, Ed. by Yu. M. Milekhin and V. A. Sorokin (Fizmatlit, Moscow, 2010) [in Russian].
2. A. Gany and D. W. Netzer, "Combustion Studies of Metallized Fuels for Solid-Fuel Ramjets," J. Propul. Power **2** (2), 423–427 (1986).
3. R. Foelsche, R. Burton, and H. Krier, "Boron Particle Ignition and Combustion at 30–150 atm," Combust. Flame **117** (1–2), 32–58 (1999).
4. A. G. Korotkikh et al., "Effect of Iron and Boron Ultrafine Powders on Combustion of Aluminized Solid Propellants," Combust. Flame **178**, 195–204 (2017).
5. S. Karmakar et al., "Effects of Rare-Earth Oxide Catalysts on the Ignition and Combustion Characteristics of Boron Nanoparticles," Combust. Flame **160** (12), 3004–3014 (2013).
6. L. Liu, P. Liu, and G. He, "Ignition and Combustion Characteristics of Compound of Magnesium and Boron," J. Therm. Anal. Calorim. **121** (3), 1205–1212 (2015).
7. J. Xi et al., "Effect of Metal Hydrides on the Burning Characteristics of Boron," Thermochim. Acta. **597**, 58–64 (2014).
8. J. Xi et al., "Metal Oxides as Catalysts for Boron Oxidation," J. Propul. Power **30** (1), 47–53 (2014).
9. P. Z. Si et al., "Amorphous Boron Nanoparticles and BN Encapsulating Boron Nano-Peanuts Prepared by Arc-Decomposing Diborane and Nitriding," J. Mater. Sci. **38** (4), 689–692 (2003).

10. J. D. Casey and J. S. Haggerty, "Laser-Induced Vapour-Phase Syntheses of Boron and Titanium Diboride Powders," J. Mater. Sci. **22** (2), 737–744 (1987).
11. A. L. Pickering et al., "Room Temperature Synthesis of Surface-Functionalised Boron Nanoparticles," Chem. Commun., No. 6, 580 (2007).
12. R. A. Yetter, G. A. Risha, and S. F. Son, "Metal Particle Combustion and Nanotechnology," Proc. Combust. Inst. **32** (2), 1819–1838 (2009).
13. E. L. Dreizin, "Metal-Based Reactive Nanomaterials," Prog. Energy Combust. Sci. **35** (2), 141–167 (2009).
14. G. Young, C. W. Roberts, and C. A. Stoltz, "Ignition and Combustion Enhancement of Boron with Polytetrafluoroethylene," J. Propul. Power **31** (1), 386–392 (2015).
15. W. Yang et al., "Impacts of Particle Size and Pressure on Reactivity of Boron Oxidation," J. Propul. Power **29** (5), 1207–1213 (2013).
16. B. E. Nikol'skii, N. L. Patratii, and Yu. V. Frolov, "Combustion of Boron-Containing Condensed Systems," Fiz. Goreniya Vzryva **28** (1), 51–53 (1992) [Combust., Expl., Shock Waves **28** (1), 45–47 (1992)].
17. A. Ulas, K. K. Kuo, and C. Gotzmer, "Ignition and Combustion of Boron Particles in Fluorine-Containing Environments," Combust. Flame **127** (1–2), 1935–1957 (2001).
18. T. L. Connell et al., "Boron and Polytetrafluoroethylene as a Fuel Composition for Hybrid Rocket Applications," J. Propul. Power **31** (1), 373–385 (2015).
19. K.-L. Chintersingh, M. Schoenitz, and E. L. Dreizin, "Oxidation Kinetics and Combustion of Boron Particles with Modified Surface," Combust. Flame **173** 288–295 (2016).
20. B. J. Bellott et al., "Nanoenergetic Materials: Boron Nanoparticles from the Pyrolysis of Decaborane and Their Functionalisation," Chem. Commun., No. 22, 3214 (2009).
21. I. Glassman, F. A. Williams, and P. Antaki, "A Physical and Chemical Interpretation of Boron Particle Combustion," Symp. Int. Combust. **20** (1), 2057–2064 (1985).
22. R. Nuzzo and G. Girolami, *High Energy Nanomaterials: Aluminum and Boron: Army Research Office Review of Nano Engineered Energetic Materials (NEEM) MURI* (HEAT Center, Aberdeen, 2010).
23. C. P. Talley, "Combustion of Elemental Boron," Aero/Space Engineering **18**, 37–47 (1959).
24. A. Maceic and J. M. Semple, "Combustion of Boron Particles at Atmospheric Pressure," Combust. Sci. Technol. **1** (3), 181–191 (1969).
25. *Burning of Powdered Metals in Active Media*, Ed. by P. F. Pokhil et al. (Nauka, Moscow, 1972) [in Russian].
26. *Ignition and Combustion of Powdered Metals*, Ed. by D. A. Yagodnikov (Bauman Moscow State Tech. Univ., Moscow, 2009) [in Russian].
27. W. Ao, J. H. Zhou, W. J. Yang, et al., " Ignition, Combustion, and Oxidation of Mixtures of Amorphous and Crystalline Boron Powders," Fiz. Goreniya Vzryva **50** (6), 51–53 (2014) [Combust., Expl., Shock Waves **50** (6), 45–47 (2014)].
28. A. S. Nechepurenko, V. M. Shamrikov, Yu. Ya. Lasychenkov, et al., "Boron, Its Oxygen-Free Compounds, and Their Application in Modern Technology," Tr. Ural. Nauch.-Issled. Khim. Inst. **72**, 1–6 (2005).
29. A. Jain et al., "Characterization of Electrodeposited Elemental Boron," Mater. Charact. **59** (7), 890–900 (2008).
30. A. Jain et al., "Structural Characterization of Electrodeposited Boron," Bull. Mater. Sci. **36** (7), 1323–1329 (2013).
31. B. Callmer, "An Accurate Refinement of the β-Rhombohedral Boron Structure," Acta Crystallogr. B **33** (6), 1951–1954 (1977).
32. S. Brutti et al., "Synchrotron Powder Diffraction Rietveld Refinement of MgB_{20} Crystal Structure," Intermetallics **10** (8), 811–817 (2002).
33. I. Higashi, "Aluminum Distribution in the Boron Framework of γ-AlB_{12}," J. Solid State Chem. **47** (3), 333–349 (1983).
34. B. Van Devener et al., "Oxide-Free, Catalyst-Coated, Fuel-Soluble, Air-Stable Boron Nanopowder As Combined Combustion Catalyst and High Energy Density Fuel," Energy Fuels **23** (12), 6111–6120 (2009).
35. W. E. Moddeman et al., "Surface Oxides of Boron and $B_{12}O_2$ as Determined by XPS," Surf. Interface Anal. **14** (5), 224–232 (1989).
36. M. Ennaceur and B. Terreault, "XPS Study of the Process of Oxygen Gettering by Thin Films of PACVD Boron," J. Nucl. Mater. **280** (1), 33–38 (2000).
37. C. Ronning et al., "Ion Beam Synthesis of Boron Carbide Thin Films," Surf. Coat. Technol. **158–159**, 382–387 (2002).
38. P. J. Kervalishvili et al., "Hydrogen, Nitrogen, and Oxygen Behavior in Boron," J. Mater. Res. **7** (7), 1822–1828 (1992).
39. D. N. Hendrickson, J. M. Hollander, W. L. Jolly, "Core-Electron Binding Energies for Compounds of Boron, Carbon, and Chromium," Inorg. Chem. **9** (3), 612–615 (1970).
40. J. J. Pireaux et al., "High Resolution ESCA Study of Uranium Fluorides: UF4 and K2UF6," Chem. Phys. Lett. **46** (2), 215–219 (1977).
41. C. D. Wagner, "Studies of the Charging of Insulators in ESCA," J. Electron Spectrosc. Relat. Phenom. **18** (3), 345–349 (1980).
42. A. I. Grigor'ev, V. I. Sigimov, and I. D. Grigor'eva, "Ignition of a Solid Particle of Boron," Fiz. Goreniya Vzryva **10** (4), 539–542 (1974) [Combust., Expl., Shock Waves **10** (4), 467–470 (1974)].

43. A. I. Grigor'ev, I. D. Grigor'eva, and V. I. Sigimov, "Oxidation Kinetics of Boron," Fiz. Goreniya Vzryva **12** (1), 52–56 (1976) [Combust., Expl., Shock Waves **12** (1), 44–47 (1976)].
44. D. Z. Safaneev, L. Ya. Kashporov, Yu. M. Grigoriev, "Heat-Liberation Kinetics in Boron–Oxygen Interaction," Fiz. Goreniya Vzryva **17** (2), 109–114 (1981) [Combust., Expl., Shock Waves **17** (2), 210–214 (1981)].
45. M. A. Trunov et al., "Effect of Polymorphic Phase Transformations in Al_2O_3 Film on Oxidation Kinetics of Aluminum Powders," Combust. Flame. **140** (4), 310–318 (2005).
46. D. Meerov et al., "Boron Particles Agglomeration and Slag During Combustion of Energetic Condensed Systems," Phys. Procedia **72**, 85–88 (2015).